



Synthesis and characterization of amine-functionalized Fe₃O₄/Mesoporous Silica Nanoparticles (MSNs) as potential nanocarriers in drug delivery systems

Hamed Tabasi¹ · Mohammad Taqi Hamed Mosavian¹ · Majid Darroudi^{2,3} · Majid Khazaei⁴ · Alireza Hashemzadeh⁵ · Zahra Sabouri⁵

Accepted: 21 April 2022 / Published online: 4 July 2022

© The Author(s), under exclusive licence to Springer Science+Business Media, LLC, part of Springer Nature 2022

Abstract

Superparamagnetic Iron Oxide Nanoparticles (SPIONs) have shown great potential for being utilized in Nanocarriers (NCs) applications throughout the Drug Delivery System (DDS). However, there are several obstacles to make a practical magnetic NCs, such as low dispersity and high toxicity in the biological systems, and also low surface area for drug loading. In this work, magnetic NCs have been synthesized through a facile three-step process, first SPIONs were synthesized by the co-precipitation method, then decorated via mesoporous silica and finally the calcinated NCs functionalized with NH₂ by a simple process in the ethanol solvent. The structure and morphology of the as-synthesized NCs have been characterized by the usage of different analyzing methods such as XRD, FTIR, TEM, FE-SEM, and TGA. Also, the magnetic properties have been investigated by the means of VSM throughout each step of the procedure. Lastly, we have applied the technique of N₂ adsorption-desorption to observe the surface area, pore size, and volume. Besides optimal magnetization of final nanoparticles (30 emu/gr), the as-synthesized NCs claimed the high surface area and small diameter, at 371 m².g⁻¹ and 70 nm, respectively. Moreover, the functionalized NCs have demonstrated well dispersity over a day in the PBS solution. As a result, the as-prepared nanocarrier able to overcome drug delivery obstacles and used as a potential nanocarrier owing to its small diameter, high surface area/ pore volume, optimal magnetization, and well dispersity in the biological condition.

Keywords SPIONs · Mesoporous silica nanoparticles (MSNs) · Nanocarriers · NH₂-functionalization · Drug delivery

1 Introduction

In recent years, nanotechnology has introduced and offered several new methods for the fields of drug delivery and cancer therapy, since nanostructure and nonporous materials have emerged as promising NCs to be applied in drug delivery systems [1–6]. Also, different nanoparticles (NPs) have been becoming increasingly popular utilizing in a wide range of applications such as zinc oxide NPs in the solar cells [7], lithium-ion batteries [8] and water treatment [9]; metallic NPs in the biology treatment as gold-NPs [10]; organic/inorganic NPs in the medicine as miracle remediation [11]; graphene oxide in the catalytic procedures [12], and CuO NPs in agriculture [13]. As it is known, magnetic NPs are practically applied throughout different fields of photocatalytic performance [14], separation [15], photocatalysis processes [16, 17], MRI and bio-imaging [18], and

✉ Mohammad Taqi Hamed Mosavian
mosavian@mail.um.ac.ir

✉ Majid Darroudi
majiddarroudi@gmail.com; darroudim@mums.ac.ir

¹ Department of Chemical Engineering, Faculty of Engineering, Ferdowsi University of Mashhad, Mashhad, Iran

² Nuclear Medicine Research Center, Mashhad University of Medical Sciences, Mashhad, Iran

³ Department of Medical Biotechnology and Nanotechnology, Faculty of Medicine, Mashhad University of Medical Sciences, Mashhad, Iran

⁴ Metabolic Syndrome Research Center, Mashhad University of Medical Sciences, Mashhad, Iran

⁵ Applied Biomedical Research Center, Mashhad University of Medical Sciences, Mashhad, Iran

biosensors [19], hyperthermia [20], bioabsorption and drug delivery systems [21, 22]. Magnetic NPs can be decorated/functionalized/ doped via various agents such as cobalt [23], zinc [24], Mn [25], SiO₂ [26], CeO₂ [27], for different goals. For instance, Sandeep B. Somvanshi et al. [28] decorated magnetic NPs via oleic acid and zinc to return Hydrophobic NPs to hydrophilic surfaces toward cancer treatment applications. Another research utilized magnetic NPs for COVID-19 detection by designing of RNA-extraction protocol [29]. Moreover, a recent and novel application of magnetic NPs is hyperthermia tumor treatment that was introduced in several research papers [24, 25, 30–32]. In the traditional hyperthermia method, all of the body and normal cells might be affected due to increasing temperature of the body up to 41–45 °C while in the novel process the cancer cells have been treated via ferro/superparamagnetic NPs precisely with an external magnet [33]. Several papers have been published on the topic of Mesoporous Silica Nanoparticles (MSNs) as promising carriers for DDS [34, 35], due to containing excellent biocompatibility, tunable pore size, high surface area, uniformed structure, and amendable surface [36–39]. There are a variety of Fe₃O₄-coatings that had been constructed to make a link between Fe₃O₄ and surfactant for the following processes and also synthesize the mesoporous silica that exists on the surface of Fe₃O₄ [40, 41]. Relatively, it can be indicated that magnetic MSNs contain the significant potential for being applied in control drug loading and release applications [42]. Nevertheless, a better loading capacity and a more specific targeting in regards to cancer cells could be achieved by considering the surface modification of NCs with several certain groups [22, 39, 43]. The process of drug loading can be triggered through different conditions such as pH, temperature, light, ultrasound, redox activation, enzymes, and glutathione [44–48]. Furthermore, NCs can be converted into smart carriers by combining their delivery with two or more drugs (overcome multidrug resistance), which enables them to identify cancer cells at the same time [49, 50]. Chengzhong Yu et al. [51] make a cancer cell detection and increase cell uptake after hyaluronic acid decorating. This research has claimed that there is an interaction between CD44 and hyaluronic acid which caused higher cell uptake [51, 52]. The low dispersity of silica-based NCs in the biological condition is an important obstacle that researchers have been looking for functionable agents to make a high disperse nanocarrier. Several nanomaterials were introduced for this purpose such as hyaluronic acid [53], oleic acid [28], folic acid [54], and polymers [55]. In this work, magnetic NCs have been synthesized through the usage of SPIONs and mesoporous silica NPs for being applied throughout the upcoming targeted drug delivery systems in the future. We have utilized NH₂-bonding to design a stable-disperse nanocarrier in the

biological systems. Besides, high surface area and high magnetization would be practical in the biomedicine as co-delivery for cancer treatment.

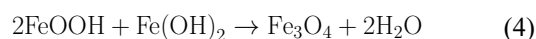
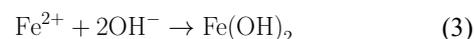
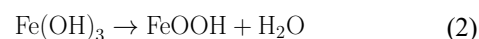
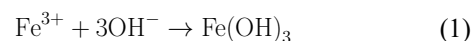
2 Experimental

2.1 Materials

Cetyltrimethylammonium bromide (CTAB), tetraethyl orthosilicate (TEOS) (98%), hydrochloric acid (HCl, 37%), sodium hydroxide (NaOH), and ethanol (99.6%) have been purchased from Sigma-Aldrich. In addition, we have procured 3-Aminopropyltriethoxysilane (APTES), ferrous chloride (FeCl₂·4H₂O, ≥99.7%), and ferric chloride hexahydrate (FeCl₃·6H₂O, ≥99.7%) from Merck (Germany), while all of the involved solutions had been prepared through the usage of ultra-pure water.

2.2 Preparation of SPIONs

SPIONs have been synthesized by the means of a co-precipitation method that had been gathered from the literature [56]. Briefly, FeCl₂·4H₂O and FeCl₃·6H₂O with the molar proportion of 1:3 have been dissolved in 12.5 mL of water, which contained 0.6 mL of HCl (37% v/v), while being under vigorous magnetic stirring within a nitrogen atmosphere. In the following, we had the temperature of the solution slowly increased to 80 °C while having it stirred for one hour and once the solution had cooled down to room temperature, 20 mL NaOH (97%) has been drop wisely added though the time of half an hour. Afterwards, the temperature of the mixture has been increased up to 80 °C for one more time and maintained for 30 min. To conclude the process, the resulting black precipitates have been collected by a magnet and washed several times with water and ethanol. The relevant reaction for the black Fe₃O₄ precipitants can be expressed as the following chemical reactions (Eq. 1 to 4) [57]:



2.3 Preparation of Fe₃O₄/MSN NCs

The as-prepared SPIONs (0.4 g) has been re-dispersed in a solution, which was consisted of 35 mL of water, 15 mL of ethanol, and 2 mL of NaOH, through the application of ultrasound for 30 min. Thereafter, 50 mL of the surfactant solution that contained 0.67 g of CTAB has been slowly and drop wisely appended into the solution while being stirred and in order to produce a homogenous colloidal suspension, the temperature of the mixture was required to be increased up to 80 °C and stirred for 4 h. As the next step, 5 mL of ethanol that was accompanied by 1 mL of TEOS has been added to the solution drop wisely and stirred for 2 h to form a dark-brown colloidal suspension. Once the mixture had been allowed to age for 18 h at room temperature, we have rapidly washed the supply with ethanol and water, which had been separated by an external magnet and dried at last. In order to collect the obtained MSN NCs, the dried colloidal NPs have been calcined at 540 °C for 6 h (heating rate: 1 °C/min) to remove the surfactant CTAB.

2.4 Preparation of amino-functionalized NCs

Fe₃O₄/MSN-NH₂ has been prepared by inducing a reaction between Fe₃O₄/MSN and APTES within ethanol. Typically, once the synthesized Fe₃O₄/MSNs (0.15 g) had been dispersed in ethanol (15 mL) and sonicated for 30 min, the APTES (200 μL) have been quickly added and stirred for 24 h at room temperature. Then, we had the Fe₃O₄/MSN-NH₂ washed by ethanol and separated through an external magnet to be dried and applied in future applications.

2.5 Characterizations

XRD patterns have been utilized to determine and confirm the materials and crystal structure, which had involved the usage of an Explorer device (GNR company, made in Italy;

diffractometer using up Cu K α radiation in 40 kV). Additionally, in order to investigate the pore structure, morphology, and particle size, we have obtained the TEM images by an LEO 912 AB (Zeiss, German) instrument with the acceleration voltage of 120 kV. FE-SEM (Philips XL-30) has been applied to characterize the particles' surface and morphology. Furthermore, FT-IR measurements have been conducted through the KBr method, while Zeta potential measurements (by Cordovan, France) have been obtained to investigate the stability of the colloidal suspension. We have also evaluated the size distribution of NPs by the means of DLS that required the usage of vasco3 (by Cordovan, France) at 25 °C and neutral pH. TGA has been performed as well through the application of a BAHF STA503 within a standard atmosphere. Lastly, the magnetic properties of these NPs have been examined in each step by the usage of a VSM.

3 Result and discussion

3.1 Nanoparticles preparation and characterization

The synthesized superparamagnetic Iron Oxide (black NPs) has been achieved through a co-precipitation method and decorated with single-layer of mesoporous silica by a sol-gel procedure in order to stabilize SPIONs besides increasing surface area and changing surface charge [58], which had been done in a basic solution that contained CTAB as a template. The observed color change is considered as another characteristic of an efficient encapsulation of SPIONs and a successful conjugation between MSNs, CTAB, and SPIONs [59]. Once the SPIONs had been encapsulated by MSNs, the color of NPs has turned to brown and became brighter as the layer of MSNs had been allowed to be thicker (by the concentration of TEOS and process time). In the following, we have performed calcination to remove the

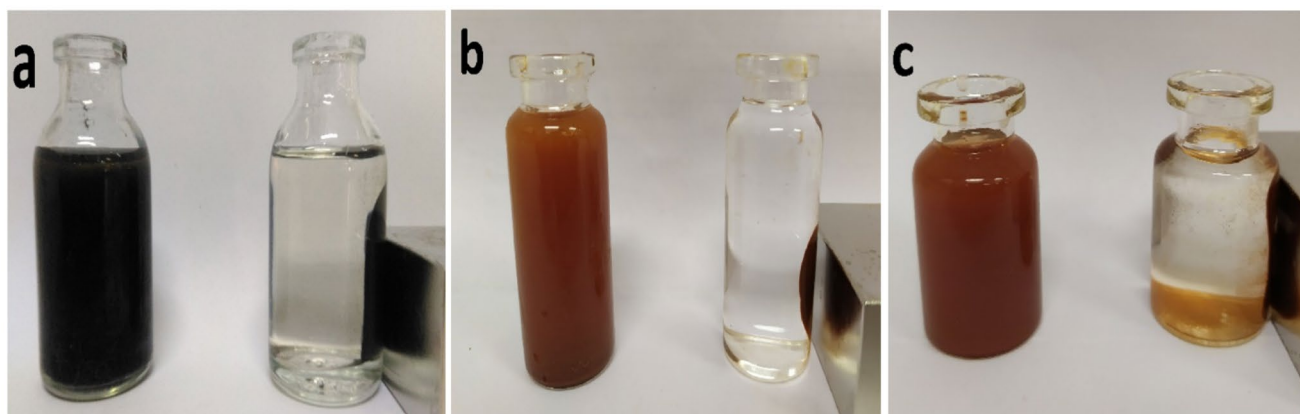


Fig. 1 The magnetization image of (a) SPIONs, (b) Fe₃O₄/MSN, and (c) Fe₃O₄/MSN-NH₂ in an external magnetic field

template, as well as to produce a porous structure and fabricate NCs. Subsequently, the surface of NCs has been functionalized with APTES (NH_2 -groups) to not only improve drug loading but also to convert the negative surface charge into a positive condition; consequently, we have absorbed a higher quantity of NCs with positive charges from cancer cells. Figure 1 demonstrates the color and magnetic properties of as-synthesized NPs.

3.2 XRD Analysis

The crystallization-structure of as-synthesized SPIONs and after performing MSN encapsulation has been characterized

Fig. 2 XRD analyze and Rietveld refinement of Fe_3O_4 , $\text{Fe}_3\text{O}_4/\text{MSN}$

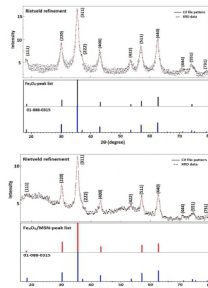


Table 1 The Rietveld refinement exploited-information for the SPIONs and $\text{Fe}_3\text{O}_4/\text{MSN}$

NPs	Phases (%)	Crystallite size (nm)
SPIONs	100	13
$\text{Fe}_3\text{O}_4/\text{MSN}$	43&57	13&67

by the utilization of XRD. Figure 2 presents the whole well-resolved diffraction peaks of the COD reference (01-088-0315) [60] which are indicative of well-crystallization with the pure phase of Fe_3O_4 NPs [61]. In comparison to the primary SPIONs, $\text{Fe}_3\text{O}_4/\text{MSN}$ has displayed broad peaks around $2\theta=20\text{--}25^\circ$ that are associated with the mesoporous structure of silica shell and the decreased intensity also claimed the encapsulated- Fe_3O_4 NPs. As can be seen from Fig. 2 some of the reference peaks such as (222), (444), and (731) (related to 18.3 , 37.1 , and 89.9°) have been appeared after the Rietveld refinement analyze while they could not be detected by the traditional methods. The Rietveld refinement analyze (Table 1) has reported the crystallite size and phases-percentage of the $\text{Fe}_3\text{O}_4/\text{MSN}$ at 13 & 67 nm and 43 & 57% respectively. This information was almost related to the matrix structure of the NCs that have been confirmed from the TEM image (Fig. 3). The diffraction peaks of 2θ at

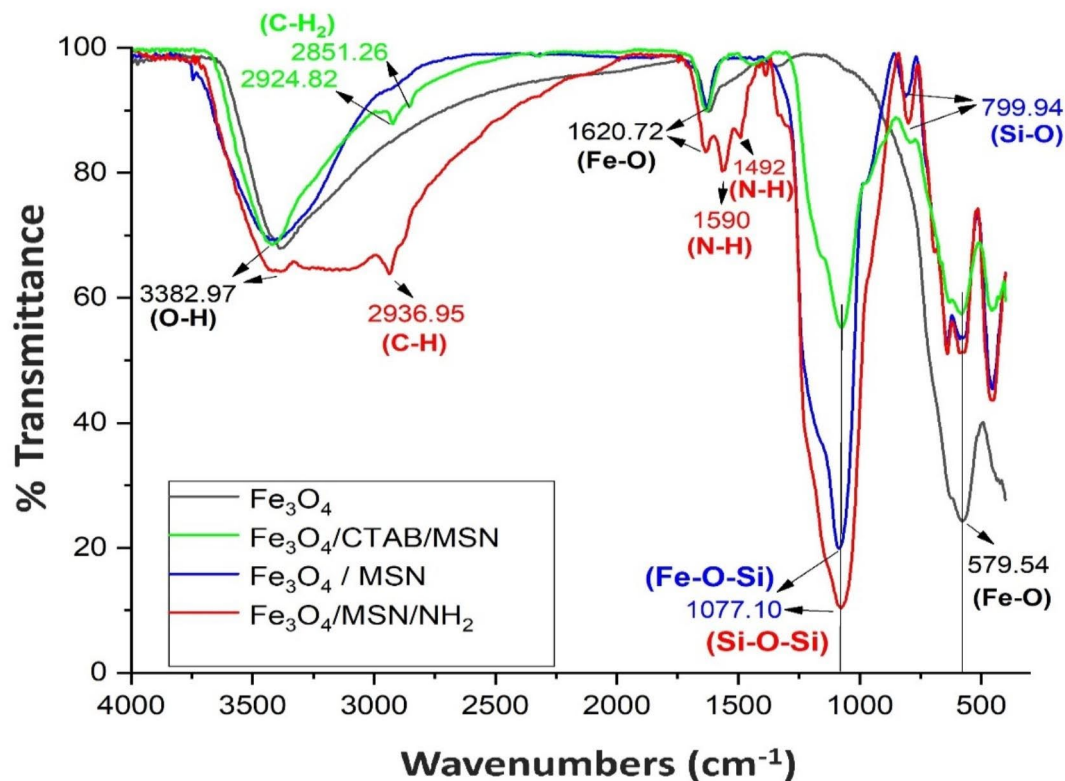


Fig. 3 Transmission Electron Microscopy (TEM) image of Silica matrix and SPIONs

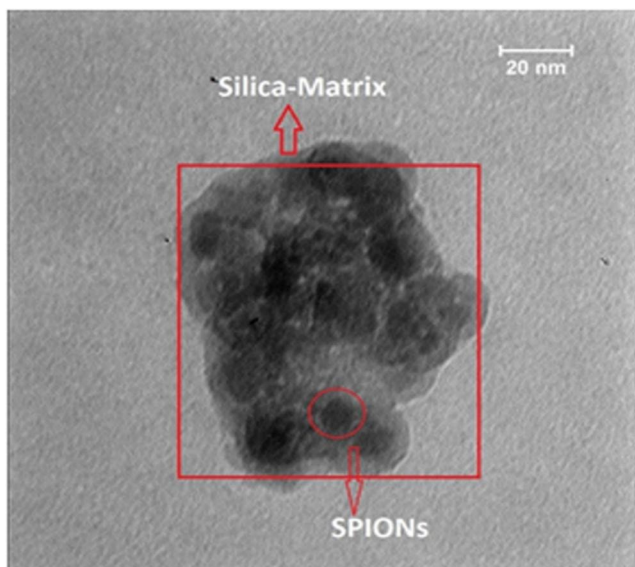


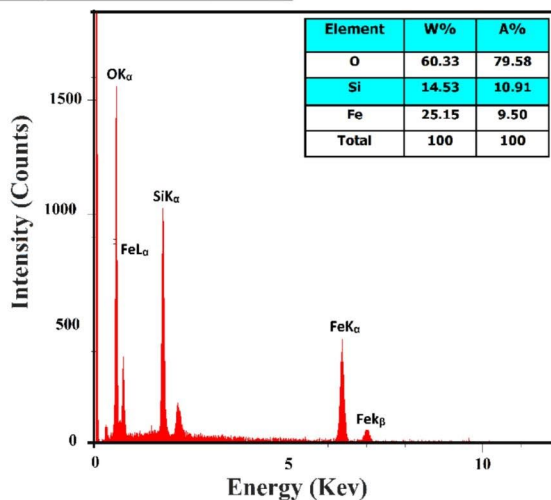
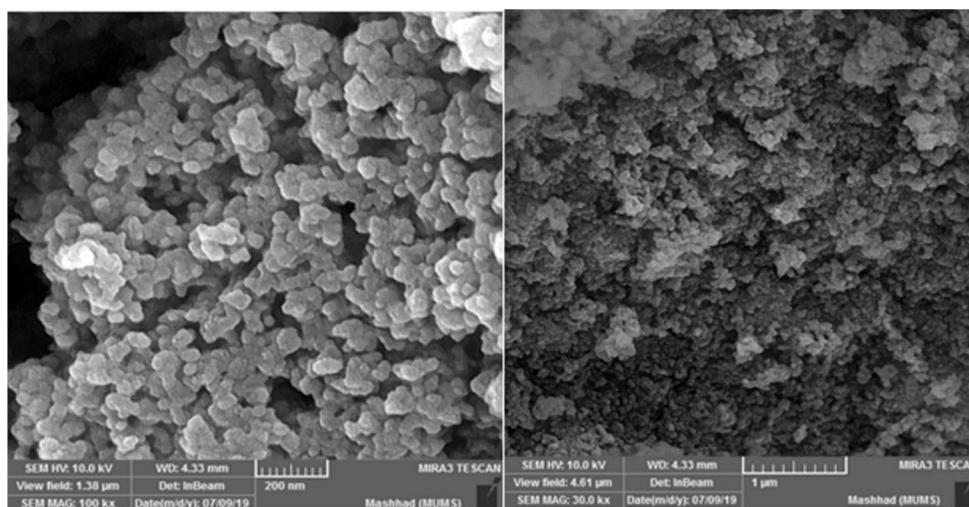
Fig. 4 FT-IR analyze of SPIONs, Fe₃O₄/MSN/CTAB, Fe₃O₄/MSN, and Fe₃O₄/MSN-NH₂

about 18.3, 37.1, and 79.1° related to (111), (222) and (444) have illustrated that the Fe₃O₄ NPs have been formed in a well-orientation because of the all necessary experimental conditions have been operated such as N₂-atmosphere from beginning to the final processes, well ions-dissolving, slow-changing pH, vigorous stirring, and vacuum-drying.

3.3 FT-IR

Figure 4 represents the FT-IR spectra of as-synthesized NPs after completing the required steps, and chemical compositions were determined by this analyze, which include SPIONs synthesis, MSN encapsulation, calcination, and functionalization. We have confirmed the formation of SPIONs by detecting the clear peaks at 579.54, and 1620.72 cm⁻¹, which are related to the stretching vibration of Fe-O [62]. The peaks at 1077.1 and 799.94 cm⁻¹ are associated with Si-O bonding and are suggestive of the fact that SPIONs have been encapsulated with MSNs through the application of CTAB template [63]. According to the FT-IR pattern that had been taken after performing calcination,

Fig. 5 Field Emission Scanning Electron Microscope (FE-SEM) with EDX images of Fe₃O₄/MSNs



the disappearance of peaks at 2924.82 and 2851.26 cm^{-1} are attributed to the deformation vibration of C–H₂ and are indicative of the complete removal of CTAB template. Finally, the NH₂-groups that had bonded on the surface of NCs have appeared at 1590, 1492 (N–H), and 2936.95 cm^{-1} (C–H) [62].

3.4 TEM/FE-SEM /EDX analysis

As it can be observed in the given TEM image (Fig. 3), the primary SPIONs are dispersed throughout the structure of MSNs, while the results have also indicated that the Fe₃O₄/MSNs had formed Fe₃O₄ as the core and MSN as the shell. It should be noted as well that the dark and lighter areas represent SPIONs and MSNs, respectively. However, although the SPIONs had been trapped within the MSNs matrix, yet the thickness of MSN layer and NPs' diameter could have been controlled by the concentration of TEOS and the duration of reaction [64]. Figure 5 presents the FE-SEM image that had been taken from the surface morphology and dispersity of Fe₃O₄/MSNs and as it can be perceived, all of the existing NPs have contained a homogeneous spherical morphology [65]. Moreover, EDX image (Fig. 5) confirms the purity of Fe₃O₄/MSN NCs without any extra element.

3.5 Zeta potential and DLS measurements

Zeta potential has been used to measure the surface charges of the as-synthesized NPs. According to the Table 2, pure SPIONs have a slight negative charge that indicates the low stability of iron oxide NPs [66]. However, by considering the Derjaguin–Landau–Verwey–O–Verbeek (DLVO) theory, their charges become more negative after being encapsulated with MSNs and consequently, their stability is empowered [67]. We have achieved the zeta potential of negative MSNs through its Surface hydroxyl groups [36]. Furthermore, the obtained data have confirmed the essential role of NCs positive charge throughout the cellular uptake of drug loading and the absorption in cancer cells. The zeta potential of Fe₃O₄/MSN has been observed to turn from negative to positive once the surface of MSN had been conjugated with NH₂-groups. We have applied the DLS analysis to examine and determine the average hydrodynamic size of NPs and for this purpose, each nanoparticle has been re-dispersed within ethanol. Table 2 presents the DLS analysis data of pure SPIONs, Fe₃O₄/MSN, and NCs that had been functionalized with APTES. The SPIONs have exhibited an average particle size of about 16 nm, which had increased to 70 nm after being encapsulated with MSN; however, this number has been observed to be increased to 81 nm subsequent to being functionalized with APTES through the addition of

NH₂-groups. Moreover, Fig. 6 illustrates the particle size distribution of as-synthesized NPs.

3.6 N₂ absorption-desorption

The surface areas have been determined by N₂ absorption-desorption method in the low-pressure range, which had involved the usage of BET model, and the pore size has been also investigated by following the BJH pore size distribution. Relatively, Table 3 represents the results of N₂ absorption-desorption analysis. According to the BJH

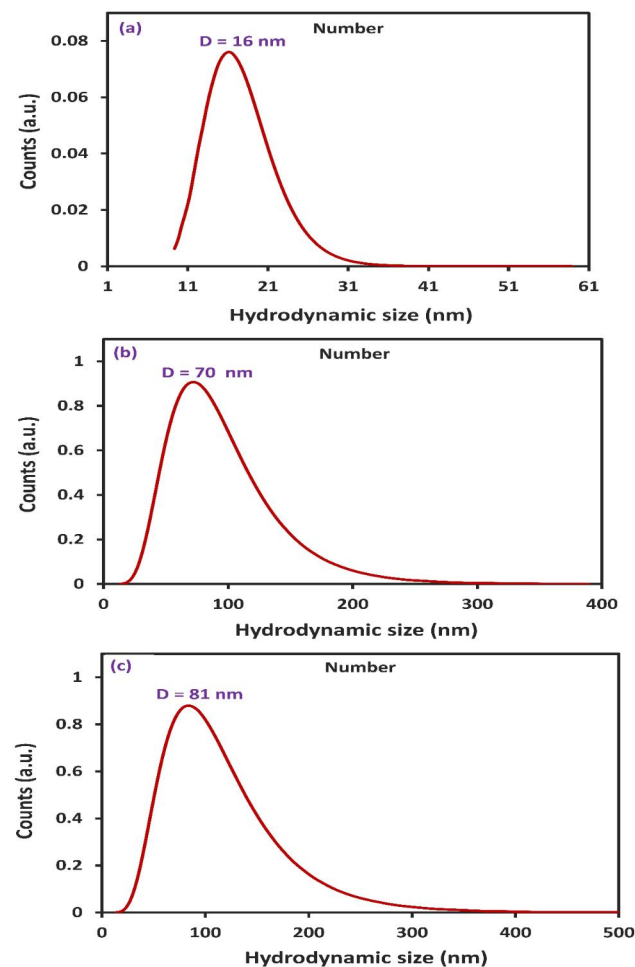


Fig. 6 Size distribution of (a) SPIONs, (b) Fe₃O₄/MSN, (c) Fe₃O₄/MSN-NH₂

Table 2 Zeta potential and DLS measurements of SPIONs, Fe₃O₄/MSN and Fe₃O₄/MSN-NH₂

NPs	SPIONs	Fe ₃ O ₄ /MSN	Fe ₃ O ₄ /MSN-NH ₂
Zeta potential (mV)	-5.5	-19.66	+18.66
Average particle size diameter(nm)	16	70	81
Polydispersity Index (PDI)	0.06	0.195	0.065

method, the surface area and cumulative pore volume have been determined to be $371 \text{ m}^2 \cdot \text{g}^{-1}$ and $404.6 \text{ cm}^3 \cdot \text{g}^{-1}$, respectively, and the average pore size has been observed to be 2.6 nm . Moreover, the modified sample has exhibited a $316 \text{ m}^2 \cdot \text{g}^{-1}$ for specific surface area, while the pore size of both cases had been the same. Even though the MSN layer was so thin, as can be seen in the Table 3 the surface area of SPIONs was risen after encapsulation by MSNs from $70 \text{ m}^2 \cdot \text{g}^{-1}$ to $371 \text{ m}^2 \cdot \text{g}^{-1}$. The N_2 adsorption-desorption isotherm for all curves (Fig. 7) illustrated the type IV isotherm whereas the $\text{Fe}_3\text{O}_4/\text{MSN}$ showed the both II and IV model (based on IUPAC Technical Report) [68] desorptions by the means it had had both nanoporous and mesoporous structure wick the nano-type pores have been blocked after NH_2 -bonding and caused to decrease the surface area to $316 \text{ m}^2 \cdot \text{g}^{-1}$. Moreover, the high surface area of non-porous SPIONs at $70 \text{ m}^2 \cdot \text{g}^{-1}$ is owing to its small nanocrystalline size ($\sim 16 \text{ nm}$). As a result, decreasing the particle's size reason to increase surface area [69]. In the other hand, the Langmuir surface area of the NCs was calculated for the maximum monolayer absorbent per gram measurement by the following formula (Eq. 5).

$$\text{Surface Area} \left(\frac{\text{m}^2}{\text{g}} \right) = \frac{X_m(\text{mg/g}) \times N \times S(\text{m}^2/\text{molecule})}{M} \quad (5)$$

Here, X_m = Maximum amount of monolayer absorbent (mg/g), M = Molecular weight of the adsorbate (mg/molecule), N = Avogadro's number and S = Contact surface area by each molecules (m^2).

Fig. 7 N_2 adsorption-desorption isotherm curves of SPIONs, $\text{Fe}_3\text{O}_4/\text{MSN}$, and $\text{Fe}_3\text{O}_4/\text{MSN-NH}_2$

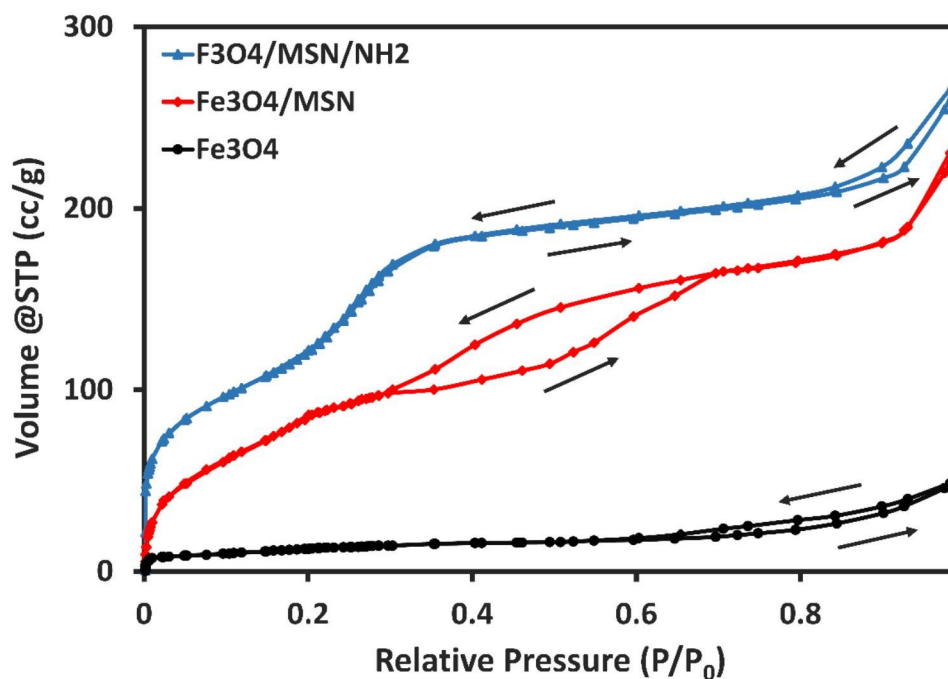


Table 3 N_2 adsorption-desorption analysis of SPIONs, $\text{Fe}_3\text{O}_4/\text{MSN}$, and $\text{Fe}_3\text{O}_4/\text{MSN-NH}_2$

Sample	BET Surface area ($\text{m}^2 \cdot \text{g}^{-1}$)	Langmuir surface area ($\text{m}^2 \cdot \text{g}^{-1}$)	Pore size (nm)	Pore volume ($\text{cm}^3 \cdot \text{g}^{-1}$)
SPIONs	70	210	-	-
$\text{Fe}_3\text{O}_4/\text{MSN}$	371	1055	2.6	0.404
$\text{Fe}_3\text{O}_4/\text{MSN-NH}_2$	316	896	2.6	0.344

3.7 TGA analysis

As it can be taken from the TGA curves (Fig. 8), the weight losses of SPIONs, $\text{Fe}_3\text{O}_4/\text{MSN}$, and $\text{Fe}_3\text{O}_4/\text{MSN-NH}_2$ as the NPs had been heated up to $1000 \text{ }^\circ\text{C}$, have been 7%, 7%, and 17%, respectively. The TGA curves of both SPIONs and $\text{Fe}_3\text{O}_4/\text{MSN}$ have displayed the high stability of NPs at high temperatures that reached up to $1000 \text{ }^\circ\text{C}$. When being compared to the curve of $\text{Fe}_3\text{O}_4/\text{MSN-NH}_2$, it can be stated that only 10% of the total modified NCs structure has belonged to the NH_2 groups. This low-percentage of NH_2 shows that a little of the surface is occupied, and this result has been obtained due to the usage of ethanol as a solvent instead of toluene (toluene is usually used as a solvent throughout the process of functionalization [22, 70–72]). The ethanol solvent contains water in its structure and this impurity prevents the bonding of NH_2 -groups on the surface of NCs in high-percentage.

3.8 VSM measurement

The magnetic properties of the as-synthesized NCs have been measured by the utilization of VSM method. Pure

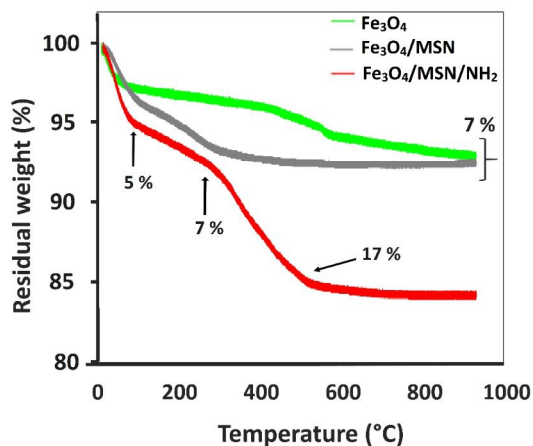


Fig. 8 TGA analysis of SPIONs, $\text{Fe}_3\text{O}_4/\text{MSN}$ and $\text{Fe}_3\text{O}_4/\text{MSN-NH}_2$

SPIONs demonstrated high saturated magnetization due to annealing-process at 80 °C for one hour (N_2 -atmosphere) [73]. The VSM results have clearly exhibited that the magnetization (MS) has decreased down to 30 and 25 emu/gr

after being encapsulated and functionalized, respectively (Fig. 9). This optimal magnetization subsequent to performing encapsulation has been caused by the none-extra Fe_3O_4 -coating whereas, in other researches, it is reported that this amount has decreased to under ten or even near-zero magnetizations [74, 75]. There have not been any signs of coercivity or superparamagnetic behaviour at room temperature throughout the curves of $\text{Fe}_3\text{O}_4/\text{MSN}$ and $\text{Fe}_3\text{O}_4/\text{MSN-NH}_2$. In addition, we have not detected any hysteresis loop or remanence in regards to $\text{Fe}_3\text{O}_4/\text{MSN}$ and $\text{Fe}_3\text{O}_4/\text{MSN-NH}_2$, which further supports the superparamagnetic properties of both of the NPs.

3.9 The advantages of NH_2 -bonding

Despite the promising application of MSNs in the field of DDS, the occurrence of aggregation in physiological situations stands as the primary obstacle that limits their implementation in nanomedicine [76]. However, the solution to this problem could be the functionalization of MSNs

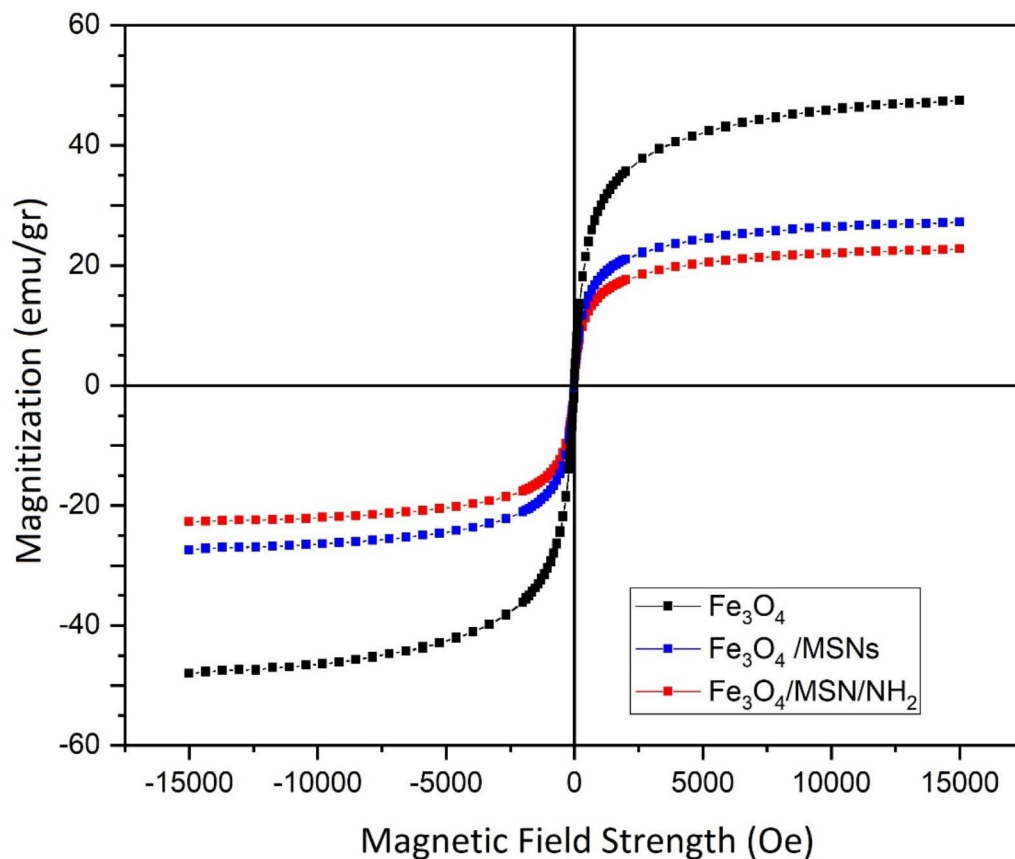


Fig. 9 Vibrating Sample Magnetometer VSM curves of SPIONs, $\text{Fe}_3\text{O}_4/\text{MSN}$ and $\text{Fe}_3\text{O}_4/\text{MSN-NH}_2$

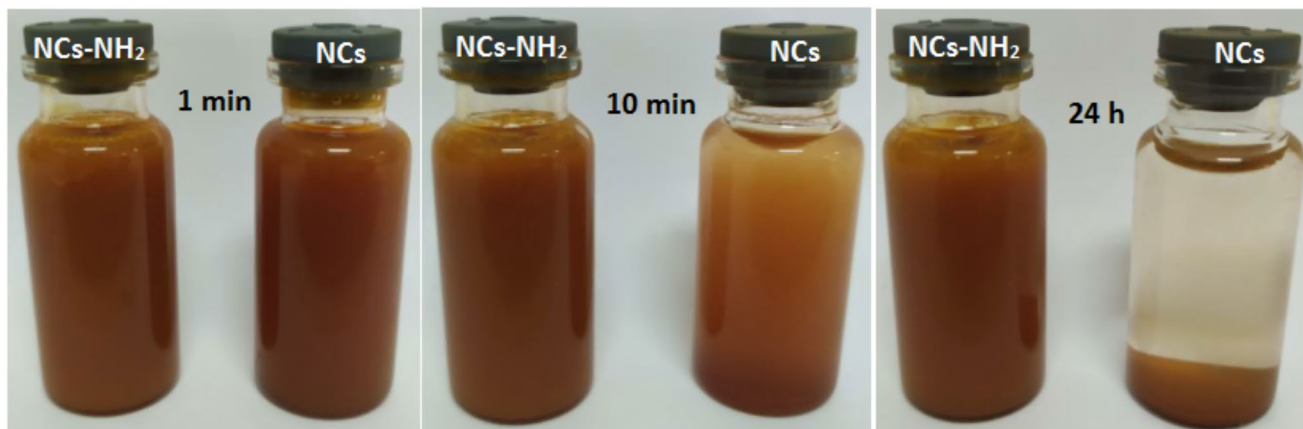


Fig. 10 Images of NCs-NH₂ and NCs (1 mg/ mL) dispersed in PBS (pH 7.4)

surface by NH₂-group. Figure 10 provides the gathered data on the stability and compatibility of functionalized NPs in suspended conditions after 24 h, whereas the not modified MSN in a similar situation had begun to aggregate after 10 min and these NPs have completely precipitated on the bottom of the glass over a day. The observed decrease in the polydispersity index (PDI) of the MSN before and after functionalization have also confirmed the inducement of an increase in stability and dispersity (Table 2).

4 Conclusion and prospective features

In this study, we have tried to prepare small NCs that would simultaneously contain high surface area and high magnetization and for this purpose, NPs have been synthesized with a thin layer of MSN and usage of well-dispersed (PDI 0.06) primary SPIONs (without any extra Fe₃O₄-coating). The ultimate size of NCs has been observed and reported to be about 80 nm, along with a 371 m².g⁻¹ surface area. We have functionalized the as-prepared NCs by APTES for conjugated NH₂ groups and according to the results, the occurrence of NH₂-bonding has increased the suspension stability in regards to physiological situations (PBS, pH 7.4). This promising design able to promote different application as hyperthermia treatment and drug release systems based on pH and electromagnetic responsive also it might be potential in the wave adsorbance application due to its magnetic/SiO₂ structure. The as-synthesized SPIONs with high magnetization properties can be utilized for the multi/nanocomposite for furthermore applications. Another interesting suggestion is that we can synthesize the SPIONs through the MOF structure to produce a novel magnetic-MOF structure. Finally, after several repeating of Fe₃O₄ synthesizing we have found that the experimental circumstance is a pivotal aspect in order to produce fine and high

magnetic powder such as N₂-atmosphere from beginning to the final processes, well ions-dissolving, slow-changing pH, vigorous stirring, and vacuum-drying.

Acknowledgements The authors gratefully acknowledge the technical support for this work provided by Ferdowsi University of Mashhad and Mashhad University of Medical Sciences based on the M. Sc thesis of Hamed Tabasi.

Author contributions Hamed Tabasi: Writing original draft, Data acquisition, analysis and interpretation. Mohammad Taqi Hamed Mosavian: Data acquisition, analysis and interpretation, review and editing, Funding and resources acquisition. Majid Darroudi: Supervision, Project administration, review & editing, Funding and resources acquisition. Majid Khazaei: Data curation, Writing - review & editing, Alireza Hashemzadeh: Data curation, Writing - review & editing. Zahra Sabouri: Data curation, Writing - review & editing.

Funding Not applicable.

Availability of data and material Not applicable.

Declarations

Conflicts of interest/competing interests The authors have declared no conflict of interest.

Ethics approval For this type of study, the ethical approval was not.

References

1. Y. Wang, D. Yao, Y. Zheng, A review on synthesis and application of solvent-free nanofluids. *Adv. Compos. Hybrid Mater.* **2**, 608–625 (2019)
2. M. Ul-Islam, J. Ali, W. Khan, A. Haider, N. Shah, M.W. Ahmad, M.W. Ullah, G. Yang, *Fast 4-nitrophenol Reduction Using Gelatin Hydrogel Containing Silver Nanoparticles* (Engineered Science, 2020)
3. S. Ghahari, E. Ghafari, P. Hou, N. Lu, *Hydration Properties of Cement Pastes with Al-Zinc Oxide and Zinc Oxide Nanoparticles* (ES Materials & Manufacturing, 2018)

4. U.K.H. Bangi, R.S. Gafari, R.C. Pawar, H.-N.-R. Jung, H.-H. Park, *Influence of Glycerol Additive on the Chemical Structure, Hydrophobicity, Morphology and Optical Properties of Sol-gel Based Zirconia Coatings* (ES Materials & Manufacturing, 2020)
5. R. Chen, J. Bao, Z. Yan, X. Huang, J. Yun, X. Zeng, J. Chen, *Preparation of Transparent Dispersions with Monodispersed Ag Nanoparticles for TiO₂ Photoelectrode Materials with Excellent Photovoltaic Performance* (Engineered Science, 2019)
6. L. Doan, Y. Lu, M. Karatela, V. Phan, C. Jeffryes, T. Benson, E.K. Wujcik, *Surface Modifications of Superparamagnetic Iron Oxide Nanoparticles with Polylactic Acid-Polyethylene Glycol Diblock Copolymer and Graphene Oxide for a Protein Delivery Vehicle* (Engineered Science, 2019)
7. S. Angaiah, S. Arunachalam, V. Murugadoss, G. Vijayakumar, *A Facile Polyvinylpyrrolidone Assisted Solvothermal Synthesis of Zinc Oxide Nanowires and Nanoparticles and Their Influence on the Photovoltaic Performance of Dye Sensitized Solar Cell* (ES Energy & Environment, 2019)
8. X.-C. Zhao, P. Yang, L.-J. Yang, Y. Cheng, H.-Y. Chen, H. Liu, G. Wang, V. Murugadoss, S. Angaiah, Z. Guo, *Enhanced Electrochemical Performance of Cu₂ + doped TiO₂ Nanoparticles for Lithium-ion Battery* (ES Materials & Manufacturing, 2018)
9. B. Jain, A. Hashmi, S. Sanwaria, A.K. Singh, M.A.B.H. Susan, A. Singh, Zinc oxide nanoparticle incorporated on graphene oxide: an efficient and stable photocatalyst for water treatment through the Fenton process. *Adv. Compos. Hybrid Mater.* **3**, 231–242 (2020)
10. Y. Xu, Y. Li, L. Wei, H. Liu, J. Qiu, L. Xiao, *Attenuation of the Aggregation and Neurotoxicity of Amyloid Peptides with Neurotransmitter-Functionalized Ultra-Small-Sized Gold Nanoparticles* (Engineered Science, 2019)
11. Q. Hu, J.-Y. Lee, Y. Luo, *Nanoparticles Targeting Hepatic Stellate Cells for the Treatment of Liver Fibrosis* (Engineered Science, 2019)
12. N. Li, F. Zhang, H. Wang, S. Hou, *Catalytic Degradation of 4-Nitrophenol in Polluted Water by Three-Dimensional Gold Nanoparticles/Reduced Graphene Oxide Microspheres* (Engineered Science, 2019)
13. J. Vassell, Y. Mao, *Effects of CuO Nanoparticles on the Growth of Kale* (ES Materials & Manufacturing, 2019)
14. Q.-Y. Li, K.-R. Ma, Z.-J. Ma, Q. Wei, J.-G. Liu, S.-P. Cui, Z.-R. Nie, Preparation and enhanced photocatalytic performance of a novel photocatalyst: Hollow network Fe₃O₄/mesoporous SiO₂/TiO₂ (FST) composite microspheres. *Microporous Mesoporous Mater.* **265**, 18–25 (2018)
15. C. Meng, W. Zhikun, L. Qiang, L. Chunling, S. Shuangqing, H. Songqing, Preparation of amino-functionalized Fe₃O₄@mSiO₂ core-shell magnetic nanoparticles and their application for aqueous Fe³⁺ removal. *J. Hazard. Mater.* **341**, 198–206 (2018)
16. B. Liu, Y. Jin, G. Xie, Z. Wang, H. Wen, N. Ren, D. Xing, *Simultaneous Photo Catalysis of SiC/Fe O Nano-particles and Photoformentation of 3 4 Rhodospseudomonas sp. nov. Strain A7 for Enhancing Hydrogen Production under Visible Light Irradiation* (ES Energy & Environment, 2018)
17. Z. Sabouri, A. Akbari, H.A. Hosseini, M. Khatami, M. Darroudi, Egg white-mediated green synthesis of NiO nanoparticles and study of their cytotoxicity and photocatalytic activity, *Polyhedron*, (2020) 114351
18. P. Zhou, J. Wang, X. Du, T. Huang, P.D. Nallathamby, L. Yang, W. Zou, Y. Zhou, J.-M. Jault, S. Chen, F. Ding, *Nanoparticles in Biomedicine-Focus on Imaging Applications* (Engineered Science, 2018)
19. L. Gao, L. Zhang, X. Lyu, G. Lu, Q. Liu, *Corrole functionalized iron oxide nanocomposites as enhanced peroxidase mimic and their application in H₂O₂ and glucose colorimetric sensing* (Engineered Science, 2018)
20. P. Das, M. Colombo, D. Proserpi, , *Biointerfaces, Recent advances in magnetic fluid hyperthermia for cancer therapy. Colloids and surfaces. B* **174**, 42–55 (2019)
21. X. Yao, X. Niu, K. Ma, P. Huang, J. Grothe, S. Kaskel, Y. Zhu, Graphene Quantum Dots-Capped Magnetic Mesoporous Silica Nanoparticles as a Multifunctional Platform for Controlled Drug Delivery, Magnetic Hyperthermia, and Photothermal Therapy, *Small*, **13** (2017)
22. E. Yu, I. Galiana, R. Martinez-Manez, P. Stroeve, M.D. Marcos, E. Aznar, F. Sancenon, J.R. Murguia, P. Amoros, *Poly(N-isopropylacrylamide)-gated Fe₃O₄/SiO₂-core shell nanoparticles with expanded mesoporous structures for the temperature triggered release of lysozyme. Colloids and surfaces*, **135** (B, Biointerfaces, 2015), pp. 652–660
23. S.B. Kale, S.B. Somvanshi, M.N. Sarnaik, S.D. More, S.J. Shukla, K.M. Jadhav, Enhancement in surface area and magnetization of CoFe₂O₄ nanoparticles for targeted drug delivery application, *1953* (2018) 030193
24. S.R. Patade, D.D. Andhare, S.B. Somvanshi, P.B. Kharat, S.D. More, K.M. Jadhav, Preparation and characterisations of magnetic nanofluid of zinc ferrite for hyperthermia. *Nanomaterials and Energy* **9**, 8–13 (2020)
25. S.R. Patade, D.D. Andhare, S.B. Somvanshi, S.A. Jadhav, M.V. Khedkar, K.M. Jadhav, Self-heating evaluation of superparamagnetic MnFe₂O₄ nanoparticles for magnetic fluid hyperthermia application towards cancer treatment. *Ceram. Int.* **46**, 25576–25583 (2020)
26. C. Yang, W. Guo, L. Cui, N. An, T. Zhang, G. Guo, H. Lin, F. Qu, Fe₃O₄@mSiO₂ core-shell nanocomposite capped with disulfide gatekeepers for enzyme-sensitive controlled release of anti-cancer drugs. *J. Mater. Chem. B* **3**, 1010–1019 (2015)
27. A. Gogoi, M. Navgire, K.C. Sarma, P. Gogoi, Fe₃O₄-CeO₂ metal oxide nanocomposite as a Fenton-like heterogeneous catalyst for degradation of catechol. *Chem. Eng. J.* **311**, 153–162 (2017)
28. S.B. Somvanshi, P.B. Kharat, M.V. Khedkar, K.M. Jadhav, Hydrophobic to hydrophilic surface transformation of nano-scale zinc ferrite via oleic acid coating: Magnetic hyperthermia study towards biomedical applications. *Ceram. Int.* **46**, 7642–7653 (2020)
29. S.B. Somvanshi, P.B. Kharat, T.S. Saraf, S.B. Somvanshi, S.B. Shejul, K.M. Jadhav, Multifunctional nano-magnetic particles assisted viral RNA-extraction protocol for potential detection of COVID-19, *Materials Research Innovations*, (2020) 1–6
30. S.B. Somvanshi, R.V. Kumar, J.S. Kounsalye, T.S. Saraf, K.M. Jadhav, Investigations of structural, magnetic and induction heating properties of surface functionalized zinc ferrite nanoparticles for hyperthermia applications, *2115* (2019) 030522
31. S.B. Somvanshi, S.R. Patade, D.D. Andhare, S.A. Jadhav, M.V. Khedkar, P.B. Kharat, P.P. Khirade, K.M. Jadhav, Hyperthermic evaluation of oleic acid coated nano-spinel magnesium ferrite: Enhancement via hydrophobic-to-hydrophilic surface transformation. *J. Alloys Compd.* **835**, 155422 (2020)
32. P.B. Kharat, S.B. Somvanshi, P.P. Khirade, K.M. Jadhav, Induction Heating Analysis of Surface-Functionalized Nanoscale CoFe₂O₄ for Magnetic Fluid Hyperthermia toward Noninvasive Cancer Treatment. *ACS Omega* **5**, 23378–23384 (2020)
33. P.B. Kharat, S.B. Somvanshi, K.M. Jadhav, Multifunctional Magnetic Nano-platforms for Advanced Biomedical applications: A Brief Review, *Journal of Physics: Conference Series*, **1644** (2020) 012036
34. X. Li, X. Wang, G. Qian, A. Ito, Synergistical chemotherapy and cancer immunotherapy using dual drug-delivering and immunopotentiating mesoporous silica. *Appl. Mater. Today* **16**, 102–111 (2019)

35. C. Pisani, E. Rascol, C. Dorandeu, C. Charnay, Y. Guari, J. Chopineau, J.-M. Devoisselle, O. Prat, Biocompatibility assessment of functionalized magnetic mesoporous silica nanoparticles in human HepaRG cells, *Nanotoxicology*, **11** (2017) 871–890
36. S. Irajli, F. Ganji, L. Rashidi, Surface modified mesoporous silica nanoparticles as sustained-release gallic acid nano-carriers. *J. Drug Deliv. Sci. Technol.* **47**, 468–476 (2018)
37. C.H. Tsai, J.L. Vivero-Escoto, I.I. Slowing, I.J. Fang, B.G. Trewyn, V.S. Lin, Surfactant-assisted controlled release of hydrophobic drugs using anionic surfactant templated mesoporous silica nanoparticles. *Biomaterials* **32**, 6234–6244 (2011)
38. A. Farooq, A. Shukur, C. Astley, L. Tosheva, P. Kelly, D. Whitehead, M. Azzawi, Titania coating of mesoporous silica nanoparticles for improved biocompatibility and drug release within blood vessels. *Acta Biomater.* **76**, 208–216 (2018)
39. S. Shahabi, S. Doscher, T. Bollhorst, L. Treccani, M. Maas, R. Dringen, K. Rezwani, Enhancing Cellular Uptake and Doxorubicin Delivery of Mesoporous Silica Nanoparticles via Surface Functionalization: Effects of Serum, *ACS applied materials & interfaces*, **7** (2015) 26880–26891
40. Y. Li, L. Liu, H. Wu, C. Deng, Magnetic mesoporous silica nanocomposites with binary metal oxides core-shell structure for the selective enrichment of endogenous phosphopeptides from human saliva. *Anal. Chim. Acta* **1079**, 111–119 (2019)
41. S. Smulders, A. Ketkar-Atre, K. Luyts, H. Vriens, S. De Sousa Nobre, C. Rivard, K. Van Landuyt, S. Baken, E. Smolders, L. Golanski, M. Ghosh, J. Vanoirbeek, U. Himmelreich, P.H. Hoet, Body distribution of SiO₂-Fe₃O₄ core-shell nanoparticles after intravenous injection and intratracheal instillation, *Nanotoxicology*, **10** (2016) 567–574
42. H. Tabasi, M.T. Hamed Mosavian, Z. Sabouri, M. Khazaei, M. Darroudi, pH-responsive and CD44-targeting by Fe₃O₄/MSNs-NH₂ nanocarriers for Oxaliplatin loading and colon cancer treatment. *Inorg. Chem. Commun.* **125**, 108430 (2021)
43. N. Knežević, E. Ruiz-Hernández, W.E. Hennink, M. Vallet-Regí, Magnetic mesoporous silica-based core/shell nanoparticles for biomedical applications. *RSC Adv.* **3**, 9584 (2013)
44. Y. Yang, Y. Lin, D. Di, X. Zhang, D. Wang, Q. Zhao, S. Wang, Gold nanoparticle-gated mesoporous silica as redox-triggered drug delivery for chemo-photothermal synergistic therapy. *J. Colloid Interface Sci.* **508**, 323–331 (2017)
45. N. Yuan, S. Li, G. Li, Sodium alginate coated mesoporous silica for dual bio-responsive controlled drug delivery. *J. Drug Deliv. Sci. Technol.* **46**, 348–353 (2018)
46. Q. Gan, X. Lu, Y. Yuan, J. Qian, H. Zhou, X. Lu, J. Shi, C. Liu, A magnetic, reversible pH-responsive nanogated ensemble based on Fe₃O₄ nanoparticles-capped mesoporous silica. *Biomaterials* **32**, 1932–1942 (2011)
47. P.-J. Chen, S.-H. Hu, C.-S. Hsiao, Y.-Y. Chen, D.-M. Liu, S.-Y. Chen, Multifunctional magnetically removable nanogated lids of Fe₃O₄-capped mesoporous silica nanoparticles for intracellular controlled release and MR imaging. *J. Mater. Chem.* **21**, 2535–2543 (2011)
48. Z. Xu, S. Liu, Y. Kang, M. Wang, Glutathione- and pH-responsive nonporous silica prodrug nanoparticles for controlled release and cancer therapy. *Nanoscale* **7**, 5859–5868 (2015)
49. B. Dutta, N.G. Shetake, B.K. Barick, K.C. Barick, B.N. Pandey, K.I. Priyadarsini, P.A. Hassan, *pH sensitive surfactant-stabilized Fe₃O₄ magnetic nanocarriers for dual drug delivery*, *Colloids and surfaces*, **162** (B, *Biointerfaces*, 2018), pp. 163–171
50. P. Zhao, L. Li, S. Zhou, L. Qiu, Z. Qian, X. Liu, X. Cao, H. Zhang, TPGS functionalized mesoporous silica nanoparticles for anticancer drug delivery to overcome multidrug resistance, *Materials science & engineering. C Mater. Biol. Appl.*, **84** (2018) 108–117
51. Z. Fang, X. Li, Z. Xu, F. Du, W. Wang, R. Shi, D. Gao, Hyaluronic acid-modified mesoporous silica-coated superparamagnetic Fe₃O₄ nanoparticles for targeted drug delivery. *Int. J. Nanomed.* **14**, 5785–5797 (2019)
52. C. Yang, W. Guo, N. An, L. Cui, T. Zhang, R. Tong, Y. Chen, H. Lin, F. Qu, Enzyme-sensitive magnetic core-shell nanocomposites for triggered drug release. *RSC Adv.* **5**, 80728–80738 (2015)
53. Q. Zhao, J. Liu, W. Zhu, C. Sun, D. Di, Y. Zhang, P. Wang, Z. Wang, S. Wang, Dual-stimuli responsive hyaluronic acid-conjugated mesoporous silica for targeted delivery to CD44-overexpressing cancer cells. *Acta Biomater.* **23**, 147–156 (2015)
54. P. Khosravian, M. Shafiee Ardestani, M. Khoobi, S.N. Ostad, F.A. Dorkoosh, H. Akbari Javar, M. Amanlou, Mesoporous silica nanoparticles functionalized with folic acid/methionine for active targeted delivery of docetaxel. *Oncotargets Ther* **9**, 7315–7330 (2016)
55. C. Lu, S. Sandoval, T. Puig, X. Obradors, G. Tobias, J. Ros, S. Ricart, Novel Fe₃O₄@GNF@SiO₂ nanocapsules fabricated through the combination of an in situ formation method and SiO₂ coating process for magnetic resonance imaging. *RSC Adv.* **7**, 24690–24697 (2017)
56. J. Zhang, X. Li, J.M. Rosenholm, H.C. Gu, Synthesis and characterization of pore size-tunable magnetic mesoporous silica nanoparticles. *J. Colloid Interface Sci.* **361**, 16–24 (2011)
57. S.M. Joshi, S. De Britto, S. Jogaiah, S. Ito, Mycogenic selenium nanoparticles as potential new generation broad spectrum antimicrobial molecules. *Biomolecules* **9**, 419 (2019)
58. J. Yu, L. Sun, *Facile One-pot Synthesis of Silver Nanoparticles Supported on α -Zirconium Phosphate Single-Layer Nanosheets* (ES Materials & Manufacturing, 2019)
59. X. Chen, H. Sun, J. Hu, X. Han, H. Liu, Y. Hu, ., *Biointerfaces, Transferrin gated mesoporous silica nanoparticles for redox-responsive and targeted drug delivery*, *Colloids and surfaces*, **152** (B, 2017), 77–84
60. T. Neuberger, B. Schöpf, H. Hofmann, M. Hofmann, B. Von Rechenberg, Superparamagnetic nanoparticles for biomedical applications: possibilities and limitations of a new drug delivery system. *J. Magn. Magn. Mater.* **293**, 483–496 (2005)
61. S.A. Jadhav, S.B. Somvanshi, M.V. Khedkar, S.R. Patade, K.M. Jadhav, Magneto-structural and photocatalytic behavior of mixed Ni-Zn nano-spinel ferrites: visible light-enabled active photodegradation of rhodamine B. *J. Mater. Sci.: Mater. Electron.* **31**, 11352–11365 (2020)
62. I. Karimzadeh, M. Aghazadeh, M.R. Ganjali, T. Doroudi, P.H. Kolivand, Preparation and characterization of iron oxide (Fe₃O₄) nanoparticles coated with polyvinylpyrrolidone/polyethylenimine through a facile one-pot deposition route. *J. Magn. Magn. Mater.* **433**, 148–154 (2017)
63. Z. Bahrami, A. Badiie, F. Atyabi, Surface functionalization of SBA-15 nanorods for anticancer drug delivery. *Chem. Eng. Res. Des.* **92**, 1296–1303 (2014)
64. T. Leshuk, H. Krishnakumar, F. Gu, Size-Tunable Fe₃O₄ Spherical Nanoclusters Through a One-Pot Hydrothermal Synthesis. *J. Nanosci. Nanotechnol.* **15**, 5378–5383 (2015)
65. Z. Sabouri, A. Akbari, H.A. Hosseini, A. Hashemzadeh, M. Darroudi, Eco-Friendly Biosynthesis of Nickel Oxide Nanoparticles Mediated by Okra Plant Extract and Investigation of Their Photocatalytic, Magnetic, Cytotoxicity, and Antibacterial Properties, *Journal of Cluster Science*, (2019) 1–10
66. S.T. Danalıoğlu, ŞS. Bayazit, Ö Kerkez, B.G. Alhogbi, M. Abdel Salam, Removal of ciprofloxacin from aqueous solution using humic acid- and levulinic acid- coated Fe₃O₄ nanoparticles. *Chem. Eng. Res. Des.* **123**, 259–267 (2017)
67. V. Bertolino, G. Cavallaro, G. Lazzara, S. Milioto, F. Parisi, Biopolymer-Targeted Adsorption onto Halloysite Nanotubes in

- Aqueous Media. *Langmuir: the ACS journal of surfaces and colloids* **33**, 3317–3323 (2017)
68. M. Thommes, K. Kaneko, A.V. Neimark, J.P. Olivier, F. Rodriguez-Reinoso, J. Rouquerol, K.S.W. Sing, Physisorption of gases, with special reference to the evaluation of surface area and pore size distribution (IUPAC Technical Report), *Pure and Applied Chemistry*, **87** (2015) 1051–1069
 69. S.B. Somvanshi, S.A. Jadhav, M.V. Khedkar, P.B. Kharat, S.D. More, K.M. Jadhav, Structural, thermal, spectral, optical and surface analysis of rare earth metal ion (Gd³⁺) doped mixed Zn–Mg nano-spinel ferrites. *Ceram. Int.* **46**, 13170–13179 (2020)
 70. L. Dong, H. Peng, S. Wang, Z. Zhang, J. Li, F. Ai, Q. Zhao, M. Luo, H. Xiong, L. Chen, Thermally and magnetically dual-responsive mesoporous silica nanospheres: preparation, characterization, and properties for the controlled release of sophoridine, *Journal of Applied Polymer Science*, **131** (2014) n/a-n/a
 71. L.B.d.O. Freitas, L.d.M. Corgosinho, J.A.Q.A. Faria, V.M. dos Santos, J.M. Resende, A.S. Leal, D.A. Gomes, E.M.B.d. Sousa, Multifunctional mesoporous silica nanoparticles for cancer-targeted, controlled drug delivery and imaging. *Microporous Mesoporous Mater.* **242**, 271–283 (2017)
 72. M.P. Shirani, B. Rezaei, T. Khayamian, M. Dinari, F.H. Shamili, M. Ramezani, M. Alibolandi, Ingenious pH-sensitive etoposide loaded folic acid decorated mesoporous silica-carbon dot with carboxymethyl- β -cyclodextrin gatekeeper for targeted drug delivery and imaging, *Materials Science and Engineering: C*, **92** (2018) 892–901
 73. Y. An, S. Feng, G. Shao, W. Yuan, K. Sun, X. Li, R. Fan, Influence of the annealing process on magnetic performance of iron based soft magnetic composites, *Engineered Science*, (2020)
 74. C. Tao, Y. Zhu, Magnetic mesoporous silica nanoparticles for potential delivery of chemotherapeutic drugs and hyperthermia. *Dalton Trans.* **43**, 15482–15490 (2014)
 75. V. Patsula, L. Kosinova, M. Lovric, L. Ferhatovic Hamzic, M. Rabyk, R. Konefal, A. Paruzel, M. Slouf, V. Herynek, S. Gajovic, D. Horak, *Superparamagnetic Fe₃O₄ Nanoparticles: Synthesis by Thermal Decomposition of Iron(III) Glucuronate and Application in Magnetic Resonance Imaging*, **8** (ACS applied materials & interfaces, 2016), pp. 7238–7247
 76. L.-S. Wang, L.-C. Wu, S.-Y. Lu, L.-L. Chang, I.T. Teng, C.-M. Yang, J.-a.A. Ho, Biofunctionalized Phospholipid-Capped Mesoporous Silica Nanoshuttles for Targeted Drug Delivery: Improved Water Susceptibility and Decreased Nonspecific Protein Binding, *ACS nano*, **4** (2010) 4371–4379

Publisher's note Springer Nature remains neutral with regard to jurisdictional claims in published maps and institutional affiliations.